JOURNAL OF CATALYSIS 107, 263–274 (1987)

EXAFS Characterization of Ru/Al_2O_3 Catalysts Using Synchrotron Radiation

G. VLAIC,* J. C. J. BART,* W. CAVIGIOLO,* A. FURESI,† V. RAGAINI,‡ M. G. CATTANIA SABBADINI,§ AND E. BURATTINI¶

*Istituto Donegani S.p.A., Via Fauser 4, 28100 Novara, Italy; †Istituto di Chimica Fisica, Università di Sassari, Via Vienna 2, 07100 Sassari, Italy; ‡Dipartimento di Chimica Fisica ed Elettrochimica, Università di Milano, Via Golgi 19, 20133 Milano, Italy; §Centro del CNR, c/o Dipartimento di Chimica Fisica ed Elettrochimica, Università di Milano, Italy; and ¶CNR and INFN, Laboratori Nazionali di Frascati, 00044 Frascati, Italy

Received October 14, 1985; revised March 2, 1987

The morphology of ruthenium catalysts, prepared from Ru-acetylacetonate [$Ru(acac)_3$] as precursor on γ-Al_2O_3 at 1.16 wt% of Ru, has been studied by EXAFS, XPS, and oxygen chemisorption techniques. $Ru(acac)_3$-impregnated γ-Al_2O_3 has been variously reduced with hydrogen at 200, 300, or 400°C for 4 or 8 h. All samples treated at 200°C show incomplete Ru reduction while for the sample treated at 300°C for 4 h the formation of Ru clusters is essentially complete and no further modifications are observed for longer reduction times or higher temperatures. Ru is anchored to the support probably through Ru^{n+}–O bonds. $Ru(acac)_3$ is therefore a useful precursor for obtaining Ru catalysts without contaminants in contrast with the behavior of Ru salts containing chlorine.

INTRODUCTION

Ruthenium has received considerable attention among the Group VIII metals, because it is a very active and versatile catalyst. It has been used, for example, in (i) the hydrogenolysis of paraffins and olefins (ethane, *n*-butane, isobutane, 1-butene, *n*-pentane) (*1–5*), being, with osmium, the most active among the Group VIII metals; (ii) the Fischer–Tropsch (F–T) synthesis (*6, 7*), being unique in its ability to produce high-molecular-weight polymers (*6*) and C_5–C_{12} hydrocarbons under mild conditions (*8*); and (iii) the synthesis of oxygenated compounds (ethanol, esters, acetic acid, acetaldehyde) by homogeneous catalysis using complexes, mainly carbonyls (*9–17*).

In the F–T synthesis the influence of promoters on the activity of Ru catalysts has not been studied as extensively as that with catalysts based on Fe. According to a report by Anderson (*18*) the presence of the promoters does not influence the synthesis performance of F–T Ru catalysts. It seems that larger ensembles of catalytic centers of Ru are required for F–T synthesis as compared with methanation (*19, 20*) and larger Ru particles have higher specific activities than do smaller particles for CO conversion (*8, 21, 22*). On the contrary, King (*22*) found that CH_4 production increases with increasing Ru metal particle size.

As for the influence of the Ru-precursor compound, Bossi *et al.* (*23*) found that on γ-Al_2O_3 significant differences exist in samples prepared using the following precursors: $RuCl_3 \cdot H_2O$, K_2RuCl_6, $K_2Ru(H_2O)Cl_5$, $KRuO_4$, $[Ru(NH_3)_6Cl_3]$ and $Ru(NO)(NO_3)_3$. Subsequently (*24*) it has been shown by the same group that, using $RuCl_3$ as precursor, Cl^- ions are still present on Ru/γ-Al_2O_3 samples but not on Ru/SiO_2 after hydrogen reduction at 400°C for 4 h. The presence of Cl^- ions could indicate incomplete reduction of Ru^{3+} to Ru^0 and would be in agreement with the findings of Blanchard and Charcosset (*25*) who proved that in Ru/γ-Al_2O_3 samples prepared from

0021-9517/87 $3.00

H_2RuCl_6, only 55% of Ru^{4+} has been reduced to Ru^0 after treatment with hydrogen at 500°C.

On the other hand, the presence of Cl^- ions may modify the C–O stretching frequency (*26*), increasing that at 2080 cm^{-1}; moreover, it is known (*27*) that when the C–O bond strength is affected the reactivity of CO is changed.

In view of the possible use of Ru catalysts for F–T and methanation reactions it seemed useful to us to eliminate the presence of Cl^- ions in the precursor compound to avoid both its effect on the incomplete reduction of Ru and its influence on CO adsorption.

Instead of the different compounds fulfilling this requirement already used in the literature to prepare Ru catalysts, i.e., Ru–acetate, $KRuO_4$, $Ru(NO)(NO_3)_3$, and $Ru(CO)_{12}$, we have chosen an alternative, i.e., Ru–acetylacetonate [$Ru(acac)_3$ or $Ru(C_5H_7O_2)_3$] supported on a Ketjen grade A γ-Al_2O_3 at about 1 wt% Ru.

The chosen system has been treated and reduced for different times at various temperatures so as to study the modification of the supported $Ru(acac)_3$ interaction with the support, the dispersion, and the morphology (metal surface area) of the Ru aggregates. The analyses have been performed mainly using EXAFS. As regards applications to catalysts, the EXAFS technique has been recently reviewed by Sinfelt *et al.* (*28*) and by two of the authors of the present paper (*29*).

EXPERIMENTAL

Preparation of the Catalysts

Catalysts were prepared by wet impregnation. A dark-red solution of $Ru(acac)_3$ (Engelhard) in toluene (solubility 1.7 g/100 ml) was used to impregnate γ-Al_2O_3 (Ketjen grade A; S.A. 310 m^2/g; $\bar{v}_p$ 0.5 ml/g). The choice of $Ru(acac)_3$ as the starting material was made following recognition that this compound is more easily reducible than H_2RuCl_6 on γ-Al_2O_3 (*25*) or $RuCl_3$ on γ-Al_2O_3 (*24*). The orange-colored impregnated catalyst containing 1.16 wt% Ru (from atomic absorption measurements) had been dried at 110°C for 4 h. To avoid formation of a high carbon deposit by heat treatment in an inert atmosphere following decomposition of the organic ligand (with consequent poisoning of the catalyst), or formation of volatile and toxic RuO_4 under oxidizing conditions, the impregnated product (RUIMP) was reduced directly in a H_2 flux (5 L/h) at 200, 300, and 400°C (accuracy: ±5°C) for 4 and 8 h. Samples were introduced to the furnace in Pyrex containers, which were sealed in a stream of He after reduction, to prevent contact of the catalyst with the atmosphere. Samples reduced at 200°C were orange–gray; those at 300 and 400°C were gray in color. In the following, RUXY identifies the catalysts; $X = 2$, 3, or 4 denotes the reduction temperature of 200, 300, or 400°C, respectively, and $Y = 4$ or 8 denotes the reduction time (in hours). Thus RU48 signifies a reduction temperature of 400°C for 8 h.

Physicochemical Characterization

Total surface areas were measured by the BET technique (Table 1) and the specific metal surface area by O_2 chemisorption at room temperature, according to the method of Buyanova *et al.* (*30*) (Table 2). Assuming

TABLE 1

Total Surface Area of Catalysts

Sample	BET surface area (m^2/g cat.)
RU48	300
RU44	290
RU38	297
RU34	254[a]
RU24	290

[a] This value is anomalous probably due to an experimental error.

TABLE 2

Metal Surface Characterization by Oxygen Chemisorption

Sample	Metal surface area (m^2/g cat.)		Mean diameter (Å) of crystallites			
	a	b	c	d	e	f
RU48	557.4	278.7	8.8	17.5	8.2	16.4
RU44	508.0	254.0	9.6	19.2	9.0	18.0
RU38	652.4	326.2	7.5	15.0	7.0	14.0
RU34	514.4	257.2	9.5	19.0	8.9	17.7
RU24	521.4	260.7	9.4	18.7	8.8	17.5

Note. a,c,e: Ru/O = 1.0; b,d,f: Ru/O = 0.5; c,d: cubic crystallites; e,f: hexagonal crystallites.

a cubic or hexagonal prismatic form for the Ru particles (with height equal to the maximum dimension of the base), a mean diameter can be derived. In view of controversy as to the stoichiometry of the Ru : O ratio (namely 1 : 1 (*30*) or 1 : 0.5 (*31*)) both hypotheses have been used for the evaluation of the particle dimensions (Table 2). Since the mean dimension $\bar{d}$ of the crystallites can be used to derive the mean coordination number (CN), comparison with the mean CN (= 5) value derived by EXAFS (see below) favors the Ru : O 1 : 1 hypothesis.

XPS measurements were carried out on a PHI 548 spectrometer using Mg$K\alpha$ radiation. As shown in Table 3, RU24 not only has a relatively high surface Ru content but also a high C content, indicative of incomplete decomposition of $Ru(acac)_3$ at 200°C. Results for the samples calcined at 300 and 400°C are similar, but different from those at 200°C.

TABLE 3

XPS Analyses of Ru Samples (at.%)

Sample	O	C	Al	Ru
γ-Al_2O_3	64.4	3.8	31.7	—
RUIMP	59.5	12.7	27.4	0.4
RU24	56.2	16.4	26.7	0.7
RU34	60.2	8.1	31.3	0.5
RU44	57.9	7.7	33.8	0.6

Sample preparation for EXAFS measurements was carried out so as to guarantee the best possible experimental conditions (*32–34*). These conditions were (a) the use of a stainless-steel cell for sample enclosure (so avoiding leakage problems of scattered X-rays which have not actually passed through the sample), (b) insignificant higher-order harmonics at the K-edge energy, (c) optimal μx values (μx = 2.5 for the catalyst and 1.3 for metallic Ru, $Ru(acac)_3$, and RUIMP after the edge), and (d) sample homogeneity (verified by optical microscopy; × 140). To this end finely dispersed metallic Ru (0.034 g) was ultrasonically suspended in 50 ml dry *n*-heptane (plus some drops of paraffin oil for the stabilization of the suspension) and filtered into a 10-μm Nucleopore polycarbonate membrane (total surface, 1.77 cm^2). $Ru(acac)_3$ (0.165 g) was prepared in the form of a pressed wafer (total surface, 2 cm^2). RUIMP and the reduced catalysts were introduced into a 9-mm-thick cell with 8-mm (diameter) ports fitted with 25-μm-thick airtight Kapton windows. All operations were carried out in a dry box filled with ultrapure N_2. The sample holder was not further exposed to air.

X-ray absorption spectra were collected in the 21,800- to 23,400-eV range with ΔE = 4.5 eV at the ADONE storage ring (PWA Line) at Frascati (Italy), which was operated at 1.5 GeV and with currents of 15–30 mA during the measurements, using a Si(111) channel-cut monochromator. Each data point was accumulated for 20 s and I_0 and I were recorded contemporarily by ionization chambers filled with 75 and 730 Torr Kr, respectively.

Data Handling

For a K edge, the simple backscattering theory gives the relationship between the EXAFS signal $\chi(k)$ and the structural parameters (*35*) by the expression

$$k \cdot \chi(k) = \sum_i \frac{N_i}{R_i^2} e^{-2R_i/\lambda} \cdot e^{-2\sigma_i^2 k^2} \cdot F_i(k) \cdot \sin[2kR_i + \Phi_i(k)], \quad [1]$$

where $k = \sqrt{2m[(E - E_0)\hbar^2]}$ is the photoelectron wave vector, E being the incident photon energy and E_0 the photoelectron binding energy; R_i is the average distance between the absorbing atom and the N_i neighboring atoms of the ith shell, with a rms deviation σ_i; $F_i(k)$ and $\Phi_i(k)$ are the amplitude backscattering factor and phase shift, respectively; and λ is the mean free path of the photoelectron.

We parametrized following the suggestions of Teo (*36*) in the form $\lambda = k/\Gamma$.

Data processing was carried out on a Univac 1100/20 computer, according to our standard procedures (*37, 38*).

E_0 has arbitrarily been chosen at the inflection point of the Ru K edge (E = 22119 eV). The EXAFS signals are shown in Figs. 1, 2, and 3 as a plot of $\chi(k)$ vs k.

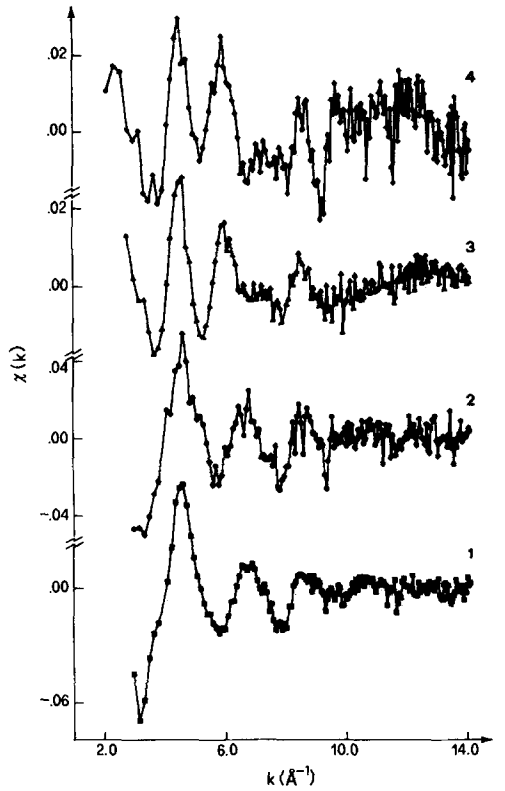

FIG. 1. $\chi(k)$ vs k EXAFS signals. Curves 1–4: Ru(acac)$_3$, RUIMP, RU24, and RU28, respectively.

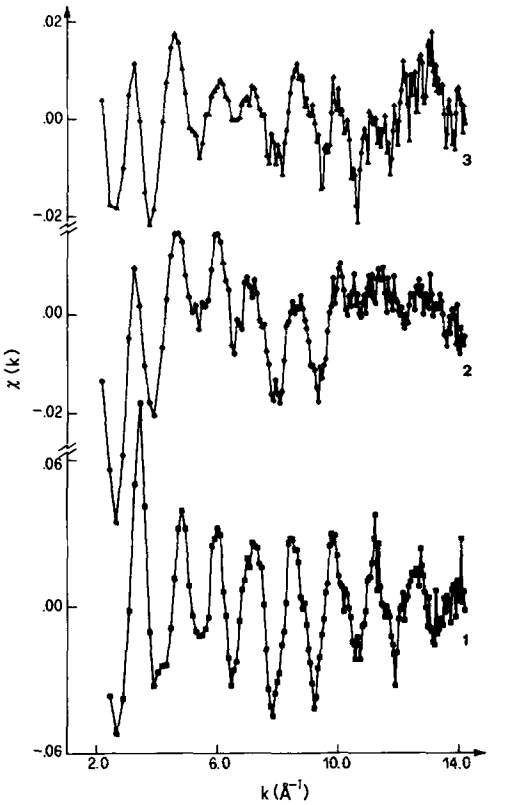

FIG. 2. $\chi(k)$ vs k EXAFS signals. Curves 1–3: Ru, RU34, and RU38, respectively.

The k^3 multiplied spectra were then Fourier-transformed from k to R space using a Hanning window (applied to the $k_{min} + \delta k_1$ and $k_{max} - \delta k_2$ ranges, with k_{min} = 3 Å^{-1}, k_{max} = 14 Å^{-1}, δk_1 = 0.5 Å^{-1}, and δk_2 = 2. Å^{-1} chosen to minimize the loss in resolution, according to the indications of Mobilio *et al.* (*39*).

Figures 4, 5, and 6 show the amplitude of the Fourier-transformed spectra |FT| vs R for the samples.

The structural parameters (i.e., N_i, R_i, and σ_i) can be obtained by a least-squares fitting of the Fourier-filtered spectra of each shell to Eq. [1], provided $F_i(k)$, $\Phi_i(k)$, and Γ are known.

The back Fourier transform (FT^{-1}) of the first shell of metallic Ru between R = 1.40

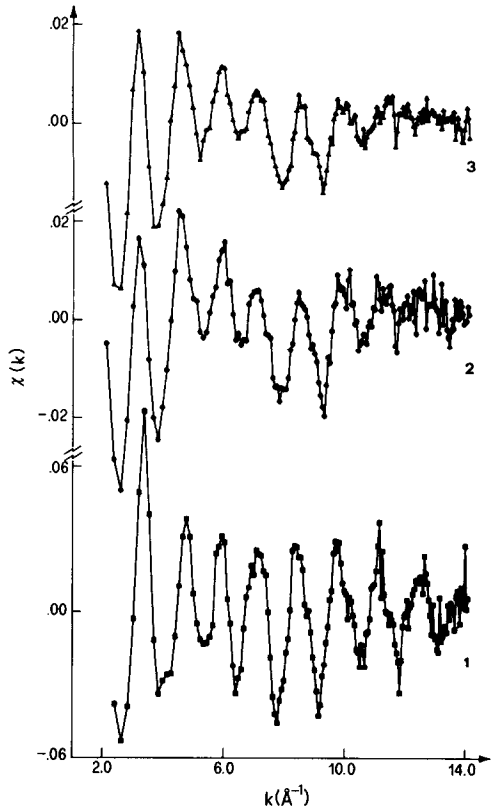

FIG. 3. $\chi(k)$ vs k EXAFS signals. Curves 1–3: Ru, RU44, and RU48, respectively.

Å and R = 2.82 Å has been utilized to evaluate the values of Γ and σ^2, using the experimental phase and the theoretical amplitude values (*40*) with N = 12, R = 2.677 Å, and ΔE = 0 eV. The fit leads to Γ = 1.566 Å and σ^2 = 0.00272 Å^2, where the latter value is similar to that reported previously by Bianconi *et al.* (*41*). The Debye–Waller factor has also been calculated with the model proposed by Sevillano *et al.* (*42*), with σ^2 = 0.0032 Å^2, in reasonable accordance with the derived experimental value. On the basis of the aforementioned parameters and using the crystallographic values for N and R, the experimental amplitudes $F(k)$ for metallic Ru have been calculated, and are compared with the theoretical values in Fig. 7. For the sake of completeness, in Fig. 8 the experimental and calculated phases of Ru are reported. It is seen that the curves are qualitatively similar in Fig. 7; for $k > 12$ Å^{-1} no comparison is possible as the experimental curve is still convoluted with the Hanning function.

Similar considerations and numerical calculations have been carried out for FT^{-1} (comprised between 1.14 and 2.12 Å) of $Ru(acac)_3$; the theoretical and experimental phases for the Ru–O absorber–backscatterer couple are more alike than those in the case of the Ru–Ru couple. The use of theoretical phases and amplitude with N = 6 leads to R = 2.01 Å, $\Delta E_0 = -12.2$ eV, Γ = 1.72 Å^{-2}, and σ^2 = 0.0012 Å^2, whereas the fit with the experimental phases and theoretical amplitudes leads to Γ = 1.70 Å^{-2} and σ^2 = 0.0011 Å^2.

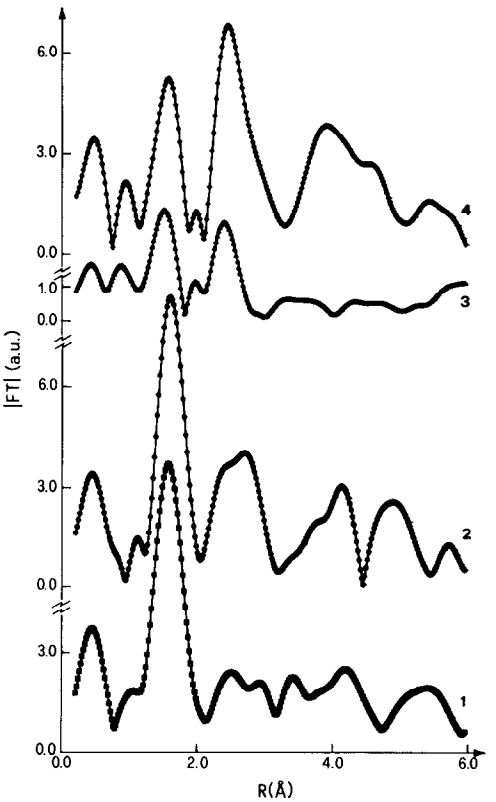

FIG. 4. Modulus of Fourier transform of Ru K-edge EXAFS spectra. See text for the limits. Curves 1–4: $Ru(acac)_3$, RUIMP, RU24, and RU28, respectively.

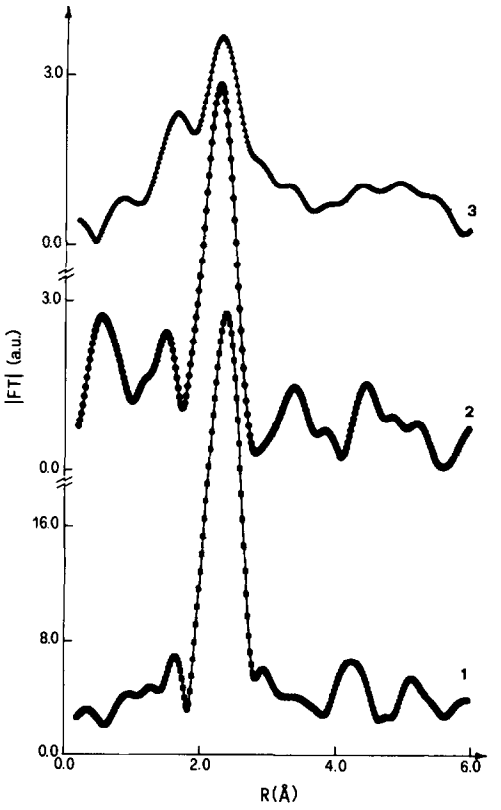

FIG. 5. Modulus of Fourier transform of Ru K-edge EXAFS spectra. See text for the limits. Curves 1–3: Ru, RU34, and RU38, respectively.

RESULTS AND DISCUSSION

Regarding metal surface characterization by oxygen chemisorption (Table 2), if we compare surface areas after a treatment of the same length, but with increasing temperatures (i.e., RU24, RU34 and RU44, or RU38 and RU48) or vice versa (i.e., RU44 and RU48) it can be observed that there is a reduction of these values; clearly this means a clustering of the metal particles with an increase in the mean diameter of crystallites, due to surface migrations. The effect, however, is small, as is proved by the greater reduction of the surface area after 8 h rather than after 4 h in the same temperature range (i.e., RU34–RU44 and RU38–RU48). Surface clustering at low temperatures (RU24–RU34) is not rare; on ruthenium it has already been observed (*43*) between room temperature and 200°C in a study on Fischer–Tropsch synthesis.

Chemisorption measurements on samples RU44 and RU48 give results which are much different from those obtained by EXAFS (see later); as regards these differences one can observe that the EXAFS technique gives first a detailed description of the distance and coordination of atoms in a cluster more than the form or size of the cluster. In this respect chemisorption measurements and EXAFS are complementary techniques.

EXAFS results are presented in Figs. 1–3. As may be seen from Fig. 2, the EXAFS of metallic Ru extends to $k \cong 14$ $Å^{-1}$ whereas the mutually quite similar spectra of $Ru(acac)_3$ and RUIMP is attrib-

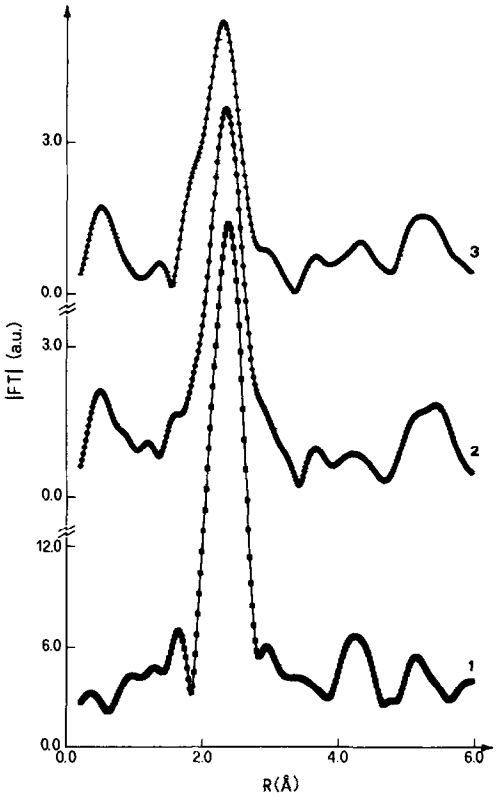

FIG. 6. Modulus of Fourier transform of Ru K-edge EXAFS spectra. See text for the limits. Curves 1–3: Ru, RU44, and RU48, respectively.

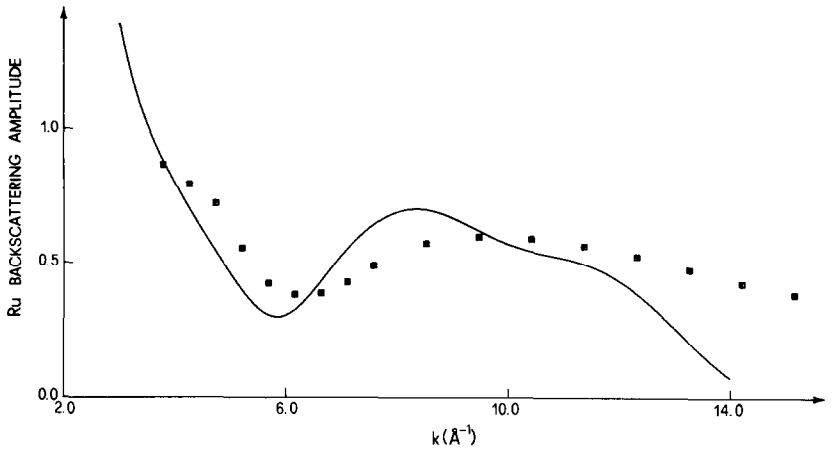

FIG. 7. Comparison between theoretical (points) and experimental (full line) amplitude functions for metallic Ru.

utable to the dilution of the sample. Catalyst samples RU24 and RU28 (Fig. 1) show quite similar frequencies but different amplitudes with damping for $k > 10$ Å^{-1}, and an appearance of "beating" in the 6- to 7.5-Å^{-1} range. Also samples RU34 and RU38 (Fig. 2) show similar frequencies (though different from Ru) but with different amplitudes in the 5- to 7.5-Å^{-1} range. In comparison with metallic Ru the variations are most significant at low k values, which is indicative of the presence of some oxygen in the coordination sphere. Catalysts RU44 and RU48 (Fig. 3) are almost identical and extend their EXAFS signals to k = 12 Å^{-1}. The observed oscillations are very similar to those of metallic Ru, though considerably reduced in amplitude.

The FT of metallic Ru is characterized by a first shell at 2.2 Å (corresponding to 6 atoms at 2.65 and 2.704 Å each (*44*)), as well as by higher shell contributions. The observed subsidiary peak at about 1.6 Å is part of the contribution to the modulus of

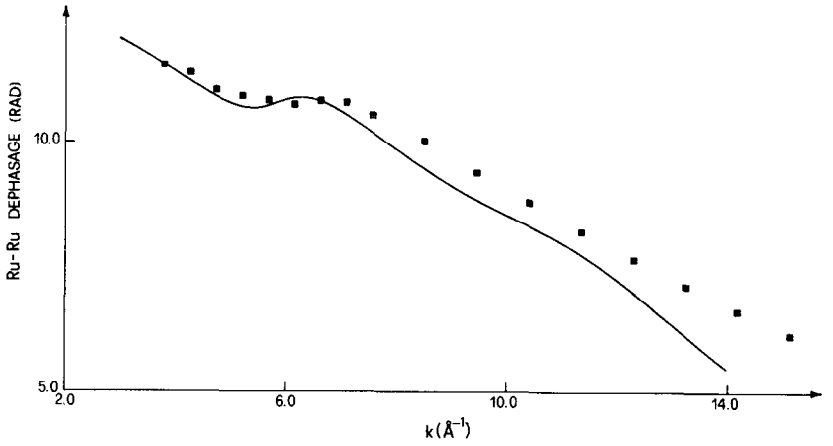

FIG. 8. Comparison between theoretical (points) and experimental (full line) phases for Ru–Ru atom pair.

the first shell as the shape of the amplitude of the scatterers (with maxima and minima) leads to doubling of the peaks in the radial distribution function (RDF) (*45*). $Ru(acac)_3$ give a RDF of the EXAFS K-edge signal with a first-shell maximum at about 1.6 Å, corresponding to six oxygen neighbors at 2.0 Å (*46*). The same situation is observed for RUIMP (Fig. 4), where maxima at higher R values are physically meaningless and due only to noise of the medium and high frequencies of the experimental signal. Catalysts RU24 and RU28 show (Fig. 4) two peaks at about 1.5 and 2.2 Å arising very probably from Ru–O and Ru–Ru contributions. The 1.5-Å peak decreases strongly in RU34 and RU38 (Fig. 5) and even more for the catalysts prepared at the highest temperature (400°C) (Fig. 6).

The catalysts and the impregnated precursor have been analyzed on the basis of the experimental amplitudes (Fig. 7) and phases (Fig. 8) of the Ru–Ru and Ru–O absorber–backscatterer pairs using a nonlinear least-squares fit on the back transform FT^{-1}. Notice that in general the EXAFS oscillations contain two sets of highly correlated variables, namely those which determine the amplitude ($F(k)$, σ^2, Γ, and N) and govern the frequency ($\phi(k)$, R, and E_0). A remedy for reducing unwanted correlations is to introduce the smallest possible number of shells, using the most accurate value for amplitude and phase and taking care of verifying good chemical sense of the calculated parameters.

The FT^{-1} of RUIMP has been calculated in the R = 1.22- to 2.04-Å range for an oxygen coordination shell. The fit (Fig. 9) leads to the parameters of Table 4, where ΔE_0 and $\Delta\sigma^2$ are referenced to $Ru(acac)_3$. The observed ΔE_0 value is less than the experimental resolution and is not indicative of modifications in the oxidation state of the metal (*47*).

TABLE 4

EXAFS Results of Ru Samples[a]

Sample	Scatterer	N	R	$\Delta\sigma^2$	ΔE_0 (eV)
RU	Ru	12.0	2.677	—	—
$RU(acac)_3$	O	6.0	2.00	—	—
RUIMP	O	6.1 ± 0.5	2.03 ± 0.01	−0.0003 ± 10%	−3.8 ± 2
RU24	Ru	5.4 ± 0.5	2.61 ± 0.03	0.0070 ± 25%	6.0 ± 2
	Ru	1.4 ± 0.5	1.96 ± 0.03	0.0114 ± 25%	14.0 ± 2
	O	2.5 ± 0.5	2.04 ± 0.03	0.0041 ± 25%	12.0 ± 2
RU28	Ru	4.9 ± 1	2.60 ± 0.05	0.0030 ± 30%	8.0 ± 4
	Ru	1.1 ± 0.5	1.98 ± 0.05	0.0020 ± 30%	11.0 ± 4
	O	1.7 ± 0.5	2.06 ± 0.05	0.0020 ± 30%	18.8 ± 4
RU34	Ru	4.8 ± 0.3	2.62 ± 0.02	0.0029 ± 15%	7.7 ± 2
	Ru	0.6 ± 0.2	1.92 ± 0.02	0.0070 ± 25%	14.9 ± 2
	O	0.5 ± 0.3	2.02 ± 0.02	—	11.0 ± 2
RU38	Ru	3.9 ± 0.5	2.62 ± 0.05	0.0030 ± 25%	6.4 ± 4
	Ru	0.4 ± 0.3	1.94 ± 0.05	0.0070 ± 30%	18.0 ± 4
	O	1.0 ± 0.5	2.02 ± 0.05	—	8.6 ± 4
RU44	Ru	4.2 ± 0.4	2.63 ± 0.02	0.0020 ± 15%	4.3 ± 2
	Ru	0.6 ± 0.2	1.96 ± 0.02	0.0090 ± 25%	12.0 ± 2
	O	0.5 ± 0.2	2.05 ± 0.02	—	2.4 ± 2
RU48	Ru	4.4 ± 0.4	2.63 ± 0.02	0.0027 ± 15%	5.7 ± 2
	Ru	0.6 ± 0.2	1.96 ± 0.02	0.0094 ± 25%	11.0 ± 2
	O	0.4 ± 0.2	2.05 ± 0.02	—	−1.5 ± 2

[a] N = coordination number; R = distance (Å); $\Delta\sigma^2$ = difference between σ^2 values of the sample and the reference $(Å)^2$.

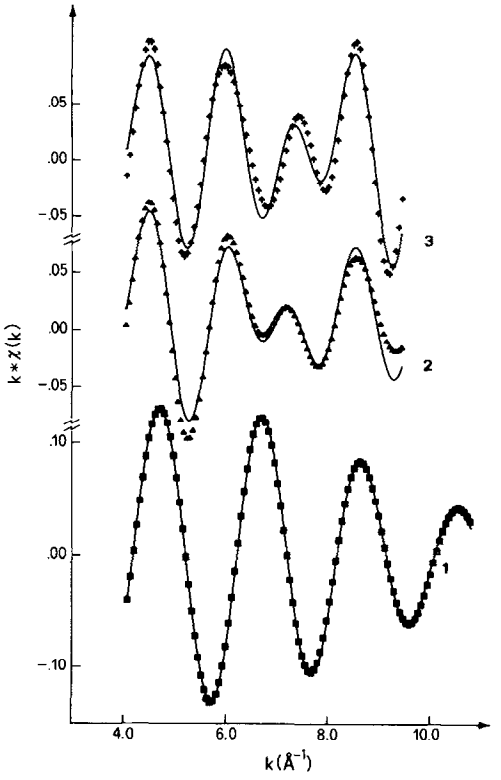

FIG. 9. Fit of $\chi(k) \cdot k$ vs k signal. Curves 1–3: RUIMP, RU24, and RU28, respectively.

The small increase in the Ru–O distance is insignificant, and also $\Delta\sigma^2$ is within the usually assumed error.

The FT^{-1} of RU44 has been calculated in the R = 1.34- to 3.40-Å range, whereas two intervals have been considered for RU48, namely R = 1.08–3.34 and 1.54–3.34 Å. A fit of the FT^{-1} of RU48 in the 1.54- to 3.34-Å range, based on a one-shell model, does not reproduce exactly the periodicity of the signal and shows considerable amplitude variation (Fig. 10). According to Bossi *et al.* (*24*), chemisorption studies of CO and H_2 on Ru/SiO_2 and Ru/Al_2O_3 are indicative of the presence of both Ru^0 and Ru^{n+} species, with a higher Ru^{n+} concentration in Ru/Al_2O_3 than that in Ru/SiO_2.

Simulation of the EXAFS signals for Ru–Ru distances of 2.63 (slightly shorter than the bulk value) and 1.97 Å shows out-of-phase features positioned exactly where the one-shell fit of RU48 was poor. These considerations allowed us to attempt a two-shell fit, with the result as indicated in Table 4. Figure 10 shows the improvement with respect to the one-shell fit; introduction of a third shell (composed of an oxygen backscatterer) from 1.08 to 3.34 Å does not lead to significant variations in the parameters of the previously defined Ru shells. For the oxygen shell (N = 0.5 at R = 2.05 Å, ΔE_0 = −1.5 eV) it has not been possible to define $\Delta\sigma^2$ because of the low coordination number, the rapid decrease in the backscattering amplitude, and the fact that the most significant effects of $\Delta\sigma^2$ on $F(k)$ are found for high k values. A completely analogous analysis was carried out

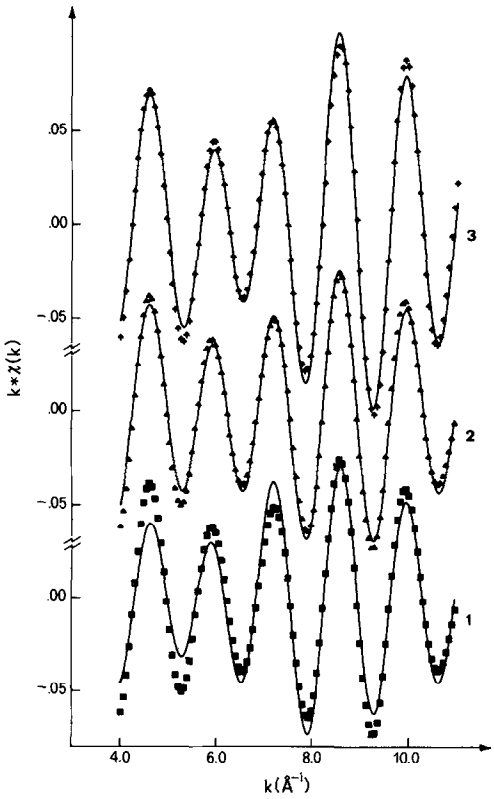

FIG. 10. Fit of the $\chi(k) \cdot k$ vs k signal for RU48 sample. Curves 1–3: one shell, two shells, and three shells, respectively.

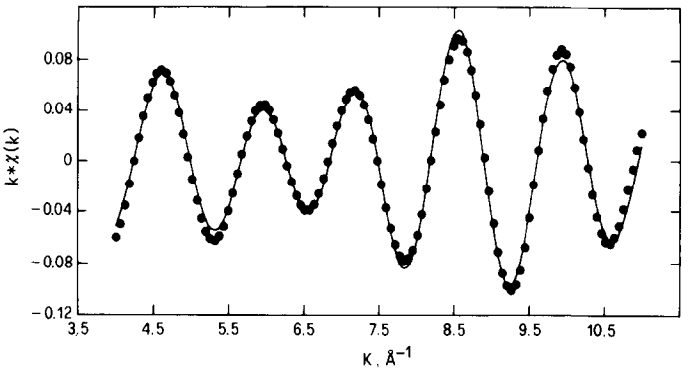

FIG. 11. Fit of the $\chi(k) \cdot k$ vs k signal for RU44 sample.

for RU44 leading to results as shown in Table 4 and Fig. 11.

Absence of any significant difference between RU44 and RU48 shows that the effect of the time of reduction at 400°C is quite small.

It has not been possible to formulate final hypotheses concerning the form of the metal clusters, due to the failure to observe higher distance shells (*48*). However, the low observed coordination number (about 5; N in Table 4) may be compared with the value of 5.5 in a close-packed (A–B–A) 13-atom cluster or 4.8 in an A–B 10-atom unit. The situation is naturally somewhat complicated by the presence of an Ru^0–Ru^{n+} contribution, but on the whole it appears that clusters at 400°C are composed of some 10–15 atoms having interactions with the oxygen of the support. Formation of monoatomic rafts is considered to be less likely because of the observed weakness of Ru–O contributions.

Spectral data for the catalysts prepared at 300°C, analyzed as above, lead to the results given in Table 4 and Fig. 12.

The final fit for RU38 is not as satisfactory as that for the others, due to the lower quality data. Therefore little significance is attached to the apparent increase in oxygen in the coordination sphere, as compared to the catalysts prepared at 400°C.

As may be seen from the estimated standard deviations, the presence of oxygen is again at the limit of significance level.

Catalysts reduced at 200°C present a considerably more complex picture than the

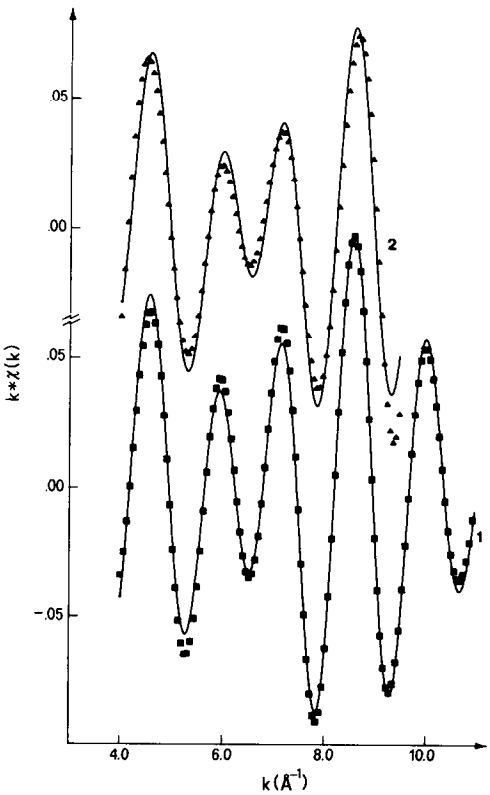

FIG. 12. Fit of the $\chi(k) \cdot k$ vs k signal for RU34 and RU38 samples.

preceding ones. As the oxygen shell is more highly populated it has been possible to define $\Delta\sigma^2$ values.

The fit for RU28 (Fig. 9) is less satisfactory than that of RU24, again reflecting the higher noise level of the raw data. RU24 is clearly a sample in an evolutionary state, where the presence of considerable amounts of Ru^0–Ru^{n+} bonds may denote nuclei of metallic ruthenium in close contact with $Ru(acac)_3$; also the orange–gray color of the sample provides an indication that not all $Ru(acac)_3$ has completely decomposed. High $\Delta\sigma^2$ values are indicative of a considerable spread in the Ru–Ru distance.

CONCLUSIONS

EXAFS data analysis of Ru/γ-Al_2O_3 catalysts indicates a high degree of dispersion of the metal, with anchoring onto the support probably through Ru^{n+}–O bonds. In catalysts prepared by reduction at 300°C in H_2 for 4 h, formation of Ru clusters is essentially complete and no further modifications are observed for longer reduction times (8 h) or higher temperatures (400°C). On the other hand, at 200°C the catalyst is in a transitional stage.

ACKNOWLEDGMENTS

One of us (A.F.) is indebted to the Istituto G. Donegani S.p.A. for kind hospitality. Thanks are due to Dr. G. Gubitosa, Dr. F. Garbassi, and Mr. R. Berté for experimental advice and to the staff of the ADONE storage ring and the PWA Laboratory (Frascati) for technical assistance.

REFERENCES

1. Sinfelt, J. H., *Catal. Rev.* **3,** 175 (1969).
2. Sinfelt, J. H., and Yates, D. J. C., *J. Catal.* **8,** 82 (1967).
3. Kempling, J. C., and Anderson, R. B., *Ind. Eng. Chem. Process Des. Dev.* **9,** 116 (1970); **11,** 146 (1967).
4. Ragaini, V., Forni, L., and Le Van Mao, R., *J. Catal.* **37,** 339 (1975).
5. Ragaini, V., Spadaro, A., and Cum, G., *React. Kinet. Catal. Lett.* **2,** 19, 135 (1975).
6. Vannice, M. A., *in* "Catalysis Science and Technology" (J. R. Anderson and M. Boudart, Eds.), Vol. 3, Chap. 3, pp. 154 and 179. Springer-Verlag, Berlin, 1981.
7. Dry, M. E., *in* "Catalysis Science and Technology" (J. R. Anderson and M. Boudart, Eds.), Vol. 1, Chap. 4, p. 194. Springer-Verlag, Berlin, 1981.
8. Everson, R. C., Woodburn, E. T., and Kirk, A. R. M., *J. Catal.* **53,** 186 (1978).
9. Warren, B. K., and Dombek, B. D., *J. Catal.* **79,** 334 (1983).
10. Knifton, J. F., *J. Catal.* **76,** 101 (1982).
11. Kellner, C. S., and Bell, A. T., *J. Catal.* **71,** 288 (1981).
12. Villeger, P., and Leclercq, G., *Bull. Soc. Chim. France* **9/10,** 406 (1979).
13. Knifton, J. F., and Grisby, R. A., *Hydrocarbon Process.* **63,** 111 (1984).
14. Knifton, J. F., Grisby, R. A., and Lin, J. J., *J. Organomet.* **3,** 62 (1984).
15. Smith, D. W., French Patent (National Distillers), 2480743, 1981.
16. Warren, B. K., U.S. Patent (UCC), 4301253, 1981.
17. Sagami Chem. Japan Kokai Tokyo Koho, Japanese Patent 82, 18639, 1982; *Appl. Catal.* **6,** 262 (1983).
18. Anderson, R. B., cited as Ref. (2) in Ref. (7).
19. Luyten, L. J. M., van Eck, M., van Grondelle, J., and van Hooff, J. H. C., *J. Phys. Chem.* **82,** 2000 (1978).
20. Dalmon, J. A., and Martin, G. A., "Proc. Intern. Congress Catalysis, 7th, Tokyo, 1980" (T. Seiyama and K. Tanabe, Eds.), p. 402. Elsevier, Amsterdam, 1981.
21. Dalla Betta, R. A., Piken, A. G., and Shelef, M., *J. Catal.* **40,** 173 (1975).
22. King, D. L., *J. Catal.* **51,** 386 (1978).
23. Bossi, A., Garbassi, F., and Tauszik, G. R., *J. Electron Spectrosc.* **13,** 145 (1978).
24. Bossi, A., Garbassi, F., Petrini, G., and Zanderighi, L., *J. Chem. Soc. Faraday Trans. I* **78,** 1029 (1982).
25. Blanchard, G., and Charcosset, H., *J. Chem. Phys.* **79,** 189 (1982).
26. Hsiu-Wei Chen, Zheng Zhong, and White, J. M., *J. Catal.* **90,** 119 (1984).
27. Ponec, V., "Spec. Per. Rep., Catalysis," Vol. 5, Chap. 2. Royal Soc. Chem., London, 1982.
28. Sinfelt, J. H., Via, G. H., and Lytle, F. W., *Catal. Rev. Sci. Eng.* **26,** 81 (1984).
29. Bart, J. C. J., and Vlaic, G., *Adv. Catal.* **35,** 1 (1987).
30. Buyanova, N. E., Karnaukhov, A. P., Koroleva, N. G., Ratner, I. D., and Chernyavskaya, O. N., *Kinet. Catal.* **13,** 1364 (1972).
31. Berté, R., Bossi, A., Garbassi, F., and Petrini, G., "7th Intern. Conf. Thermal Analysis, Kingston, Ontario" (B. Miller, Ed.), p. 1124, 1982.
32. Stern, E. A., *Phys. Rev. B* **17,** 40 (1978).

33. Goulon, J., Goulon-Ginet, C., Cortés, R., and Dubois, J. M., *J. Phys.* **43,** 539 (1982).
34. Rose, M. E., and Shapiro, M. M., *Phys. Rev.* **74,** 1853 (1948).
35. Lytle, F. W., Sayers, D. E., and Stern, E. A., *Phys. Rev. B* **11,** 4836 (1975).
36. Teo, B. K., *in* "EXAFS Spectroscopy, Technique and Applications" (B. K. Teo and D. C. Joy, Eds.), p. 21. Plenum, New York, 1981.
37. Vlaic, G., Bart, J. C. J., Cavigiolo, W., Mobilio, S., and Navarra, G., *Chem. Phys.* **64,** 115 (1982).
38. Vlaic, G., and Bart, J. C. J., *Rec. Trav. Chim.* **101,** 171 (1982).
39. Mobilio, S., Comin, F., and Incoccia, L., Lab. Naz. Frascati, Int. Report, LFN-82/19 (NT), 1982.
40. Teo, B. K., and Lee, P. A., *J. Amer. Chem. Soc.* **101,** 2815 (1979).
41. Bianconi, A., Dell'Ariccia, M., Giovannelli, A., Burattini, E., Cavallo, N., Patteri, P., Pancini, E., Carlini, C., Ciardelli, F., Papeschi, D., Pertici, P., Vitulli, G., Dalba, G., Fornasini, P., Mobilio, S., and Palladino, L., *Chem. Phys. Lett.* **90,** 257 (1982).
42. Sevillano, E., Meuth, H., and Rehr, J., *Phys. Rev. B* **20,** 4908 (1979).
43. Everson, R. C., Smith, K. Y., and Woodburn, E. T., "Proc. Ind. Mtg. S. Afr. Inst. Chem. Eng., 3rd, Stellenbosch, 1–3 April, 1980," P2D/1; see also Anderson, R. B., "The Fischer–Tropsch Synthesis," Chap. 4, p. 116, Table 10. Academic Press, New York, 1984.
44. Pearson, W. B., "A Handbook of Lattice Spacings and Structure of Metals and Alloys," p. 128. Pergamon, London, 1958.
45. Rabe, P., Tolkiehn, G., and Werner, A., *J. Phys. C* **12,** 899 (1979).
46. Chao, G. K. J., Sime, R. L., and Sime, R. J., *Acta Crystallogr. B* **29,** 2845 (1973).
47. Vlaic, G., Bart, J. C. J., Cavigiolo, W., and Mobilio, S., *Chem. Phys. Lett.* **76,** 453 (1980).
48. Lagarde, P., Murata, T., Vlaic, G., Freund, E., Dexpert, H., and Bournonville, J. P., *J. Catal.* **84,** 333 (1983).